

High material quality growth of AlInAsSb thin films on GaSb substrate by molecular beam epitaxy

Fa-Ran Chang(常发冉), Rui-Ting Hao(郝瑞亭), Tong-Tong Qi(齐通通), Qi-Chen Zhao(赵其琛), Xin-Xing Liu(刘欣星), Yong Li(李勇), Kang Gu(顾康), Jie Guo(郭杰), Guo-Wei Wang(王国伟), Ying-Qiang Xu(徐应强), Zhi-Chuan Niu(牛智川)

Citation: Chin. Phys. B . 2019, 28(2): 028503. **doi:** 10.1088/1674-1056/28/2/028503
Journal homepage: http://cpb.iphy.ac.cn; http://iopscience.iop.org/cpb

What follows is a list of articles you may be interested in

Recent advances in Ga-based solar-blind photodetectors

Ming-sheng Xu(徐明升), Lei Ge(葛磊), Ming-ming Han(韩明明), Jing Huang(黄静), Hua-yong Xu(徐化勇), Zai-xing Yang(杨再兴)

Chin. Phys. B . 2019, 28(2): 028502. **doi:** 10.1088/1674-1056/28/2/028502

Preparation of Ga_2O_3 thin film solar-blind photodetectors based on mixed-phase structure by pulsed laser deposition

Y M Lu(吕有明), C Li(李超), X H Chen(陈相和), S Han(韩瞬), P J Cao(曹培江), F Jia(贾芳), Y X Zeng(曾玉祥), X K Liu(刘新科), W Y Xu(许望颖), W J Liu(柳文军), D L Zhu(朱德亮)

Chin. Phys. B . 2019, 28(1): 018504. **doi:** 10.1088/1674-1056/28/1/018504

Review of deep ultraviolet photodetector based on gallium oxide

Yuan Qin(覃愿), Shibing Long(龙世兵), Hang Dong(董航), Qiming He(何启鸣), Guangzhong Jian(菅光忠), Ying Zhang(张颖), Xiaohu Hou(侯小虎), Pengju Tan(谭鹏举), Zhongfang Zhang(张中方), Hangbing Lv(吕杭炳), Qi Liu(刘琦), Ming Liu(刘明)

Chin. Phys. B . 2019, 28(1): 018501. **doi:** 10.1088/1674-1056/28/1/018501

Integration of a field-effect-transistor terahertz detector with a diagonal horn antenna

Xiang Li(李想), Jian-dong Sun(孙建东), Zhi-peng Zhang(张志鹏), V V Popov, Hua Qin(秦华)

Chin. Phys. B . 2018, 27(6): 068506. **doi:** 10.1088/1674-1056/27/6/068506

Performance of dual-band short- or mid-wavelength infrared photodetectors based on InGaAsSb bulk materials and InAs/GaSb superlattices

Yao-yao Sun(孙姚耀), Yue-xi Lv(吕粤希), Xi Han(韩玺), Chun-yan Guo(郭春妍), Zhi Jiang(蒋志), Hong-yue Hao(郝宏玥), Dong-wei Jiang(蒋洞微), Guo-wei Wang(王国伟), Ying-qiang Xu(徐应强), Zhi-chuan Niu(牛智川)

Chin. Phys. B . 2017, 26(9): 098506. **doi:** 10.1088/1674-1056/26/9/098506

High material quality growth of AlInAsSb thin films on GaSb substrate by molecular beam epitaxy*

Fa-Ran Chang(常发冉)[1], Rui-Ting Hao(郝瑞亭)[1,†], Tong-Tong Qi(齐通通)[1], Qi-Chen Zhao(赵其琛)[1], Xin-Xing Liu(刘欣星)[1], Yong Li(李勇)[1], Kang Gu(顾康)[1], Jie Guo(郭杰)[1,‡], Guo-Wei Wang(王国伟)[2,3,§], Ying-Qiang Xu(徐应强)[2,3], and Zhi-Chuan Niu(牛智川)[2,3]

[1] *School of Energy & Environment Science, Key Laboratory of Renewable Energy Advanced Materials and Manufacturing Technology, Ministry of Education, Yunnan Key Laboratory of Opto-electronic Information Technology, Yunnan Normal University, Kunming* 650092, *China*

[2] *State Key Laboratory for Superlattices and Microstructures, Institute of Semiconductors, Chinese Academy of Sciences, Beijing* 100083, *China*

[3] *Center of Materials Science and Optoelectronics Engineering, University of Chinese Academy of Sciences, Beijing* 100049, *China*

(Received 11 September 2018; revised manuscript received 26 November 2018; published online 10 January 2019)

In this paper, high material quality $Al_{0.4}In_{0.6}AsSb$ quaternary alloy on GaSb substrates is demonstrated. The quality of these epilayers is assessed using a high-resolution x-ray diffraction, Fourier transform infrared (FTIR) spectrometer, and atomic force microscope (AFM). The x-ray diffraction exhibits high order satellite peaks with a measured period of 31.06 Å (theoretical value is 30.48 Å), the mismatch between the GaSb substrate and AlInAsSb achieves −162 arcsec, and the root-mean square (RMS) roughness for typical material growths has achieved around 1.6 Å over an area of 10 μm ×10 μm. At room temperature, the photoluminescence (PL) spectrum shows a cutoff wavelength of 1.617 μm.

Keywords: AlInAsSb, short-wavelength, digital alloy

PACS: 85.60.Gz, 68.65.Cd, 72.20.Jv **DOI:** 10.1088/1674-1056/28/2/028503

1. Introduction

Nowadays, the short wavelength infrared (SWIR) band, from 1 μm to 3 μm, shows a broad range of applications, including telecommunication, astronomical observation, gas analysis and earth sciences. A camera that is capable of SWIR imaging will produce a higher resolution image than conventional visible infrared cameras. Besides, imaging in this band can exhibit the capacity to perform both passive and active imaging. Therefore, it has many applications in military and civilian applications. Up to now, a variety of material systems, such as HgCdTe (MCT) and InGaAs, have addressed parts of this region. However, photodetectors based on $In_xGa_{1-x}As$ compounds have some limitationd for tenability of cut-off wavelength. Their performance reduces rapidly when the cut-off wavelength is beyond 1.7 μm due to mismatch-induced defects.[1,2] Photodetectors based on HgCdTe can cover the range of 1 μm–3μm by changing the molar fraction of Cd. However, these photodetectors not only necessitate complex material growth but also need a complicated procedure for fabrication of the device, which exhibits high cost and toxicity.[3,4]

In contrast, photodetectors based on the $Al_xIn_{1-x}AsSb$ (henceforth referred to as AlInAsSb) quaternary compound are promising candidates for both optoelectronic and electronic devices due to their flexibility to tune the bandgap and band offsets of heterostructures lattice matched to InP,[5] InAs[6,7] or GaSb[8,9] substrates. Varying the aluminum content tuned the bandgap from 0.25 eV (0% aluminum) to 1.18 eV (72% aluminum), corresponding to photon wavelengths from 5 μm to 1.05 μm.[10]

This material has many advantages, such as low growth and manufacturing costs, great flexibility in bandgap engineering, and suppression of Auger recombination due to the large effective mass. Shown in Fig. 1, the material structure is alternately grown from InAs and AlSb, which can significantly reduce GR-based dark current, the trap-assisted and band-to-band tunneling. This may lead to an increase in material properties.

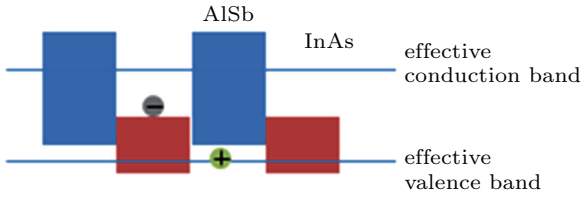


Fig. 1. The band alignment and the effective band gap in InAs/AlSb superlattice. Colored rectangles represent the forbidden band gap of the materials.

*Project supported by the National Natural Science Foundation of China (Grant Nos. 61774130 11474248, 61176127, 61006085, 61274013, and 61306013, the Key Program for International Science and Technology Cooperation Projects of China (Grant No. 2011DFA62380), and the Ph. D. Programs Foundation of the Ministry of Education of China (Grant No. 20105303120002).

†Corresponding author. E-mail: ruitinghao@semi.ac.cn

‡Corresponding author. E-mail: jieggg1020@sina.com

§Corresponding author. E-mail: wangguowei@semi.ac.cn

© 2019 Chinese Physical Society and IOP Publishing Ltd

2. Experimental methods

The $Al_{0.4}In_{0.6}AsSb$ quaternary alloy was first grown by the bulk material growth method. One of the advantages of this method is that the growth rate was greatly improved. The bulk material growth method requires that all four elements of the shutter be opened and sprayed onto the surface of the substrate. It means that the growth rate of In is 3/2 of the growth rate of Al in $Al_{0.4}In_{0.6}AsSb$. Then the tip and base temperature of Al and In was found. Finally, various growth conditions such as growth temperature and V/III ratio to achieve optimal growth parameters.

In the growth process, it was discovered that the reproducibility of growth of the bulk material was not good after repeated experiments. In order to achieve lattice matching, it takes a lot of time to re-commission the V/III beam equivalent pressure (BEP) ratio and growth temperature before each growth process. Even worse, most of the components of AlInAsSb are in a miscible gap on the GaSb substrate in a thermodynamic equilibrium state.[11] In order to solve these problems, a growth method named the digital alloy method similar to the superlattice was adopted.

The digital alloy method mainly adjusts the lattice matching by changing the thickness of each layer, it does not require the V group beam to be strictly stable. So, it improves the repeatability of the experiment. The AlSb and InAs layers mainly used in the growth of AlInAsSb are grown by the digital alloy method. However, simple calculation showed that $Al_{0.4}In_{0.6}As_{0.6}Sb_{0.4}$ was impossible to reach lattice-matching condition if only used the layer of AlSb and InAs. The average overall lattice constant

$$a(Al_{0.4}In_{0.6}As_{0.6}Sb_{0.4}) = 0.4 \times a(AlSb) + 0.6 \times a(InAs) = 6.0892 < 6.0959,$$

where

$$a(AlSb) = 6.1355\ \text{Å}, \quad a(InAs) = 6.0583\ \text{Å}, \quad a(GaSb) = 6.0959\ \text{Å}.$$

In order to achieve matching with GaSb under high Al composition and low Al composition, AlAs and InSb layers were inserted between the AlSb and InAs layers to adjust the compressive and tensile strains, respectively. These layers were grown as a digital alloy of the binary alloys AlAs, AlSb, InAs, and InSb so as to bypass the wide miscibility gap present in the $Al_xIn_{1-x}As_ySb_{1-y}$ material system, using a digital alloy period of 3 nm and the following shutter sequence: AlSb, AlAs, AlSb, Sb, In, InAs, In, and Sb.[10,12,13] To match the GaSb substrate, the shutter sequences, monolayers and time in components of Al is 0.4, as shown in Table 1.

Table 1. The shutter sequences and time in components of Al is 0.4.

Sequence	AlSb	AlAs	AlSb	Sb	In	InAs	In	Sb
Monolayer	1.87	0.26	1.87	–	0.35	5.3	0.35	–
Time/s	4.68	0.65	4.68	3	0.88	13.25	0.88	3

3. MBE growth and characteristics

All samples in this paper were grown in a solid source Gen II molecular beam epitaxy system on an n-type GaSb (001) substrate, which was equipped with valved cracker sources for group V (Sb2 and As2) fluxes and Ga, In, and Al SUMO cells. Before each growth, the high temperature was maintained for 30 minutes to remove the surface oxide,[14] and a few nanometers of GaSb buffer layer was grown at 540 °C to smooth the surface. When the Sb beam is 9.26×10^{-7} Torr (1 Torr = 1.33322×10^2 Pa), *in-situ* reflection high-energy electron diffraction (RHEED) was used to monitor the temperature at which the substrate surface transitions from 2×5 to 1×3, this transition occurred at a substrate temperature of T_c.

For all the samples, optical microscopy was used to estimate surface defects, the surface morphology was studied with a digital S–II Nano Navi atomic force microscope (AFM), the bandgap of materials was measured using a Bruker Vertex-70 Fourier transform infrared (FTIR) spectrometer and HRXRD measurement with ω–2θ scan was carried out to obtain lattice mismatch between AlInAsSb and GaSb substrate and examine the crystal quality.

The material structure utilized for both XRD studies and PL studies is shown in Table 2. First, a 20-nm GaSb buffer layer was deposited. Then, the 30-nm thick AlSb barrier layer was grown. Before the next 30-nm AlSb barrier was the 40 periods AlInAsSb superlattices. Finally, it finished by a 20-nm GaSb capping layer. The 30-nm thick AlSb barrier aided PL studies by blocking the diffusion of photo-generated carriers to the top surface and into the GaSb buffer, while the 20-nm GaSb cap protected the underlying AlSb and AlInAsSb form oxidation.

Table 2. Schematic cross-section of the material structure.

20-nm GaSb cap
30-nm AlSb barrier
40-p AlInAsSb
30-nm AlSb barrier
20-nm GaSb buffer
GaSb substrate (Te)

Three samples with the As/In BEP flux ratio of 4, 6, and 8 were grown, while the Sb/Al BEP flux ratio were 5. The high-resolution x-ray diffraction is shown in Fig. 2. By observing the lattice mismatch between the epitaxial and the substrate of the experimental samples, a phenomenon that the quality of the sample rise and then fall as the As/In BEP flux ratio risen was observed. We speculate that the suitable As/In BEP flux

ratio is about 6. The BEP flux ratio of 4 shows there are fewer AlAs interfaces in the middle of the two AlSb layers, and the BEP flux ratio of 8 shows the opposite direction. However, there are many other growth parameters which still need to be adjusted, because Figure 2(b) shows a +241.2-arcsec lattice mismatch.

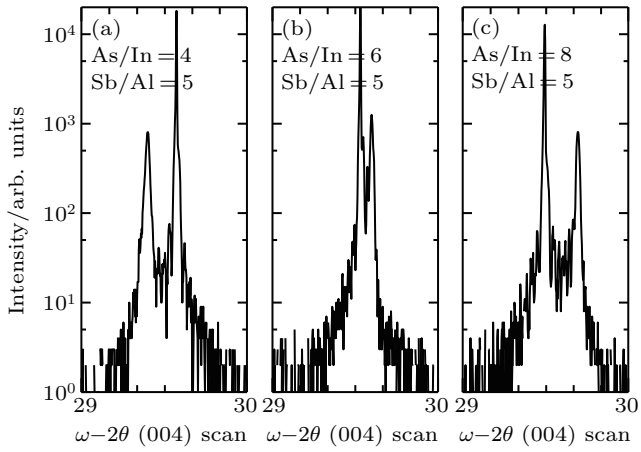


Fig. 2. The high-resolution x-ray diffraction of the three $Al_{0.4}In_{0.6}AsSb$ superlattices varied with the BEP flux ratio (a) As/In = 4, (b) As/In = 6, (c) As/In = 8. The strain and the full width at half maximum (FWHM) of samples were (a) −622.8 arcsec, 82.8 arcsec; (b) +241.2 arcsec, 57.6 arcsec; (c) +720 arcsec, 75.6 arcsec, respectively.

Optimized growth conditions for AlAs have been obtained. To achieve a zero lattice mismatch between the $Al_{0.4}In_{0.6}AsSb$ and the GaSb substrate sample, three samples with the Sb/Al BEP flux ratio of 4, 6, and 8 were grown, while the As/In BEP flux ratio were 6. The high-resolution x-ray diffraction is shown in Fig. 3. In this step, the zero lattice mismatch was achieved in Fig. 3(b), while the FWHM is 57.6 arcsec. The surface morphology of the sample is shown in Fig. 4(c), which the Sb/Al and As/In BEP flux ratio were 6 and 6, respectively. The clear pyramid protrusion defects are easy to be observed.

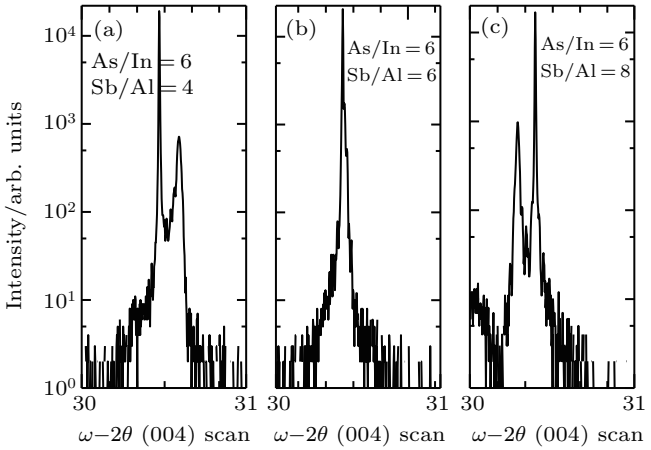


Fig. 3. The high-resolution x-ray diffraction of the three $Al_{0.4}In_{0.6}AsSb$ superlattices varied with the III/V BEP flux ratio (a) Sb/Al = 4, (b) Sb/Al = 6, (c) Sb/Al = 8. The strain and the FWHM of samples were (a) 432 arcsec, 93.6 arcsec; (b) 0 arcsec, 57.6 arcsec; (c) 378 arcsec, 64.8 arcsec, respectively.

Studies have shown that the energy of the Ehrlich–Schwoebel (ES) barrier at the surface atomic step determines the migration and desorption of high-energy atoms on the surface of the material during growth.[15,16] The growth temperature determines the energy of the ES barrier. Therefore, it is very important to optimize the growth temperature of the substrate. The purpose is to minimize the influence of the ES barrier on the surface atom migration.

In the growth of digital alloys, the optimum growth temperature is neither the best growth temperature of InAs nor the best of AlSb. The optimum growth temperature of the material is close to the optimal growth temperature of the InSb interface because it plays a main role in adjusting the stress. Excessive growth temperature will destroy the In–Sb bond, too low growth temperature is not conducive to the growth of InAs, especially AlSb layers.

A low growth temperature allows for better adhesion of the group III atoms, while a higher growth temperature favors detaching the excess group V atoms and allows better migration of surface atoms. However, the too low growth temperature is not conducive to the diffusion of the group V atoms, resulting in the atom step of the material is not obvious, and the morphology is river-like. A too high growth temperature makes the group III atoms less likely to adhere, and the surface forms pores lacking group III atoms.

Using above optimized growth parameter, the $Al_{0.4}In_{0.6}AsSb$ material was grown at $T_g = T_c - 15$ °C, $T_g = T_c$, $T_g = T_c + 15$ °C, and $T_g = T_c + 30$ °C. Then, their XRD images are shown in Fig. 4, and their AFM images are shown in Fig. 5.

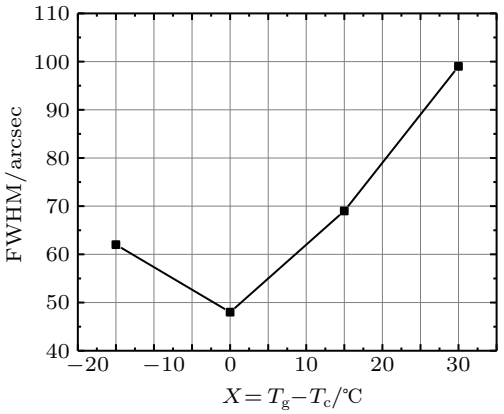


Fig. 4. FWHM value of materials at different growth temperatures.

The size of the FWHM value can indicate the growth quality of the material interface to some extent. Figure 4 shows the variation trend of FWHM values of materials at different growth temperatures. When the temperature is T_c, the FWHM value of the material is the smallest, and the FWHM of the material will increase regardless of whether the growth temperature is increased or decreased. This indicates that the material interface is flat at the growth temperature of T_c.

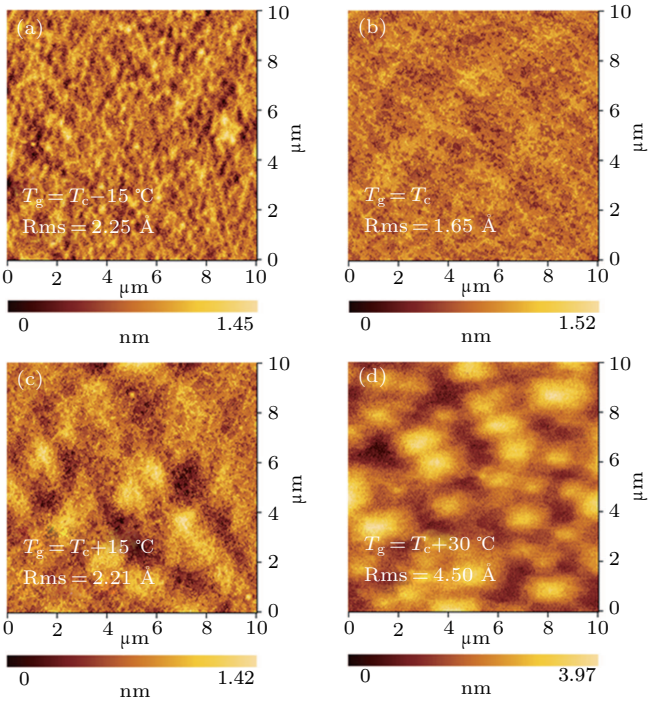


Fig. 5. AFM images of $T_c - 15$ °C (a), T_c (b), $T_c + 15$ °C, (c) and $T_c + 30$ °C (d) sample surface over 10 μm × 10 μm.

It can be seen from Fig. 5(a) that when the growth temperature is $T_c - 15$ °C, the atomic step on the surface of the material is not obvious, and it is river-like, indicating that the surface III group atoms have good adhesion, but the group V atoms have not been sufficiently diffused, so the growth temperature is low.

When the growth temperature is $T_c + 30$ °C, it can be seen from Fig. 5(d) that some pores lacking Group III atoms are formed. It is indicated that the Group V atoms are sufficiently desorbed and migrated on the surface of the material, but the Group III atoms are not sufficiently adhered, so the growth temperature is high.

When the growth temperature is T_c, a uniform water-rippled atomic step is formed on the surface of the material, which indicated that the ES barrier at this temperature makes the Group III and V atoms have the best migration and diffusion.

The period thickness and the lattice mismatch between the $Al_{0.4}In_{0.6}AsSb$ and the GaSb substrate are determined from the HRXRD measurements.[17] The measured period of this material is about 31.06 Å (theoretical value is 30.48 Å) as shown in Fig. 6, and the x-ray diffraction exhibits high order satellite peaks. The FWHM of the zeroth-order peak is about 46.8 arcsec for the device growth. On the other hand, the AFM image shows an RMS surface roughness around 1.65 Å and clear atom steps over an area of 10 μm × 10 μm. The high material quality of the $Al_{0.4}In_{0.6}AsSb$ has been achieved. In the end, the PL spectrum measurements of the $Al_{0.4}In_{0.6}AsSb$ DA were conducted at 300 K using a Fourier transform infrared (FTIR) spectrometer. The excitation source uses a semiconductor pumped solid-state laser with a power of 1 W and a laser wavelength of 671 nm, and the laser power is adjusted by an attenuator. Figure 7 shows the cutoff wavelength of 1.617 μm. This is similar to the value reported in the journal article.[10] The small peak on the right side of the main peak is the GaSb substrate peak.

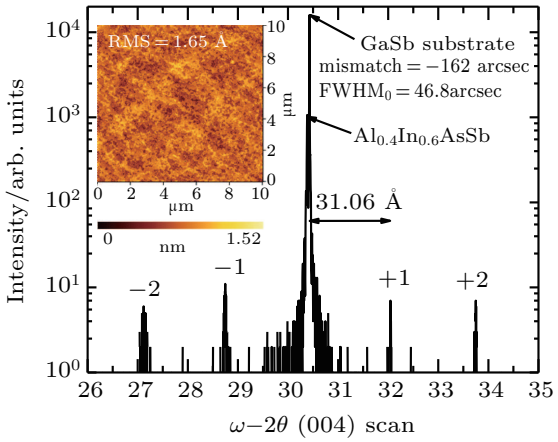


Fig. 6. High-resolution x-ray diffraction of $Al_{0.4}In_{0.6}AsSb$ superlattice using the optimized condition. (Inset: AFM image of the sample surface over 10 μm×10 μm).

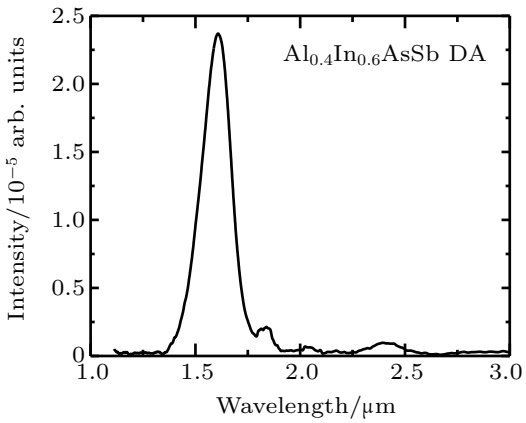


Fig. 7. PL spectrum of the $Al_{0.4}In_{0.6}AsSb$ DA.

4. Conclusion

In summary, we have shown that stable substrate temperature and optimal control of the flux ratios are of critical importance to growing high-quality AlInAsSb alloy matched to GaSb. Using the shutter sequence: AlSb, AlAs, AlSb, Sb, In, InAs, In, and Sb, the BEP flux ratio As/In and Sb/Al of 6, and the optimized growth temperature T_c, narrow FWHM and high order satellite peaks of AlInAsSb indicates that we succeed in growing high-quality AlInAsSb superlattices on the GaSb substrate. In the next step, we will fabricate AlInAsSb photodetectors by using an ICP dry etch and a standard photolithographic process to verify the promising optical and electrical characterizations.

References

[1] Gallant M, Puetz N, Zemel A and Shepherd F 1988 *Appl. Phys. Lett.* **52** 733

[2] Kozlowski L J, Arias J M, Williams G M, Vural K, Cooper D E, Cabelli S A and Bruce C 1994 *Infrared Detectors: State of the Art II*, 1994, San Diego, CA USA, pp. 93–117

[3] Tennant W, Lee D, Zandian M, Piquette E and Carmody M 2008 *J. Electron. Mater.* **37** 1406

[4] Lee D, Carmody M, Piquette E, Dreiske P, Chen A, Yulius A, Edwall D, Bhargava S, Zandian M and Tennant W 2016 *J. Electron. Mater.* **45** 4587

[5] Chang J, Su Y K, Jaw D, Shiao H and Lin W 1999 *J. Crystal Growth* **203** 481

[6] Semenov A, Solov'Ev V, Meltser B Y, Terent'ev Y V, Prokopova L and Ivanov S 2005 *J. Crystal Growth* **278** 203

[7] Zederbauer T, Andrews A M, MacFarland D, Detz H, Schrenk W and Strasser G 2016 *Photonics* **3** 20

[8] Washington-Stokes D, Hogan T P, Chow P C, Golding T D, Kirschbaum U, Littler C L and Lukic R 1999 *J. Crystal Growth* **201** 854

[9] Tournet J, Rouillard Y and Tournié E 2017 *J. Cryst. Growth* **477** 72

[10] Maddox S J, March S D and Bank S R 2016 *Cryst. Growth & Des.* **16** 3582

[11] Vaughn L G 2006 "Mid-infrared multiple quantum well lasers using digitally-grown aluminum indium arsenic antimonide barriers and strained indium arsenic antimonide wells", Ph. D. dissertation (New Mexico: University of New Mexico) (in American)

[12] Vaughn L G, Dawson L R, Pease E A, Lester L F, Xu H, Jiang Y and Gray A L 2005 *Physics and Simulation of Optoelectronic Devices XIII*, 2015, San Jose, California, USA pp. 307

[13] Lyu Y, Han X, Sun Y, Jiang Z, Guo C, Xiang W, Dong Y, Cui J, Yao Y, Jiang D, Wang G, Xu Y and Niu Z 2018 *J. Crystal Growth* **482** 70

[14] Neuberger M 2013 *III–V semiconducting compounds* (Springer Science & Business Media)

[15] Schwoebel R L and Shipsey E J 1966 *J. Appl. Phys.* **37** 3682

[16] Chiu T, Tsang W, Ditzenberger J, Chu S and Van der Ziel J 1986 *J. Appl. Phys.* **60** 205

[17] Rodriguez J, Christol P, Cerutti L, Chevrier F and Joullié A 2005 *J. Crystal Growth* **274** 6